Hindawi Publishing Corporation
Journal of Nanomaterials
Volume 2013, Article ID 785023, 14 pages
http://dx.doi.org/10.1155/2013/785023

Research Article

Characterization of Porous WO_3 Electrochromic Device by Electrochemical Impedance Spectroscopy

Chien Chon Chen

Department of Energy Engineering, National United University, Miaoli 36003, Taiwan

Correspondence should be addressed to Chien Chon Chen; chentexas@gmail.com

Received 4 October 2012; Accepted 22 December 2012

Academic Editor: Wen Zeng

This paper concerns the microstructure of the anodic tungsten oxide (WO_3) and its use in an electrochromic (EC) glass device. When voltages between 100 V and 160 V were applied to tungsten film for 1 h under 0.4 wt. % NaF electrolyte, porous WO_3 film was formed. The film, which had a large surface area, was used as electrochromic film for EC glass. The average transmittance in a visible region of the spectrum for a 144 cm^2 EC device was above 75% in the bleached state and below 40% in the colored state, respectively. Repeatability using of the colored/bleached cycles was tested good by a cyclic voltammograms method. The internal impedance values under colored and bleached states were detected and simulated using an electrical impedance spectra (EIS) technique. The EC glass impedance characteristics were simulated using resistors, capacitors, and Warburg impedance. The ITO/WO_3, WO_3/electrolyte, electrolyte/NiO, and NiO/ITO interfaces can be simulated using a resistance capacitance (RC) parallel circuits, and bulk materials such as the indium tin oxide (ITO) and conducting wire can be simulated by using a series of resisters.

1. Introduction

In recent years, the nanometer technological progress has led to the creation of many special new materials. Therefore now, information photoelectricity, catalysis, and magnetism have broader application domains because of nanotechnology. For example, the tungsten oxide (WO_3), which has rich special physics and chemical properties, is widely treated as electrochromic (EC) [1, 2].

According to a 2012 US department of energy (DOE) report, windows contribute to about 40 percent of overall building heating and cooling load with annual impact of about 4.4 quads, and there is a potential to reduce lighting impact by 1 quad through day lighting. The Environmental Protection Agency says an average household spends over 40 percent of its annual energy budget on heating and cooling costs. By 2020, industry leaders believe that windows will become active parts of building climate, engineering, information, and structural systems. Advanced electrochromic (EC) technologies such as EC windows will darken in sunlight without the use of an external control circuit. Such windows would be ideal for applications such as car sunroofs. According to the National Renewable Energy Laboratory (NREL), by allowing control of daylighting and solar gain, electrochromic windows have the potential to reduce annual US energy consumption by several quadrillion (10^{15}) Btus (quads). The United States currently consumes a total of about 94 quads of energy per year [3–5].

EC glass—also known as smart windows or switchable windows—changes its light transmission properties when voltage is applied. This type of window has "memory" and does not need constant voltage once the change has been initiated [6, 7]. The use of smart glass can allow control of the amount of light and heat passing through and thus save heating, air conditioning, and lighting costs. An EC device is comprised of five layers: the working electrode, the ion conducting layer, and the counter electrode are sandwiched between two electronically conductive transparent electrodes coated on glass. Critical aspects of smart glass include installation costs, the use of electricity, durability, as well as functional features such as the speed of control, possibilities for dimming, and the degree of transparency of the glass [8–10].

Tungsten trioxide (WO_3) has been the most widely used material in EC glass since its electrochromism was

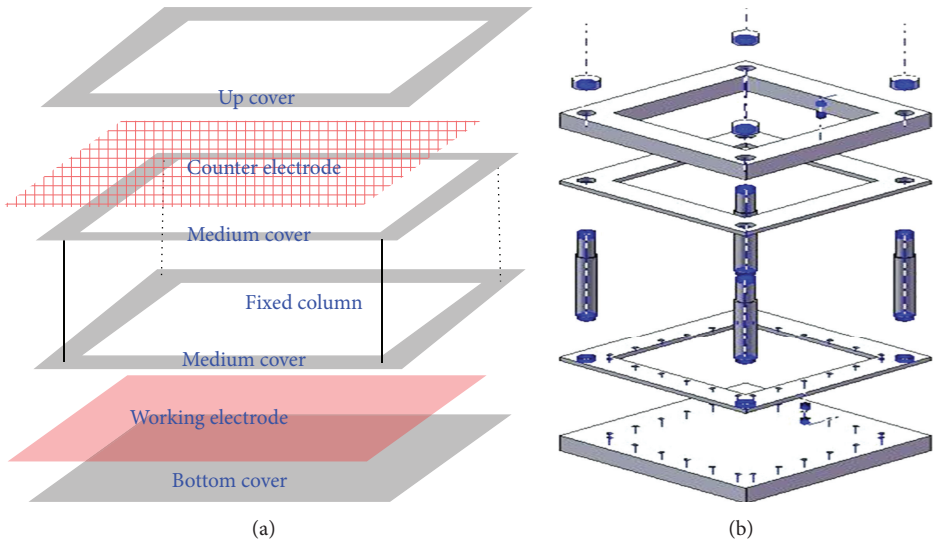

FIGURE 1: Schematic diagram of anodization mold: (a) counter electrode is fixed between top and middle cover, working electrode is between middle and bottom cover, and the counter-working electrodes distance is adjusted by using a fixed column and (b) three-dimensional diagram.

first reported in 1969 [11, 12]. Tungsten oxide has a large number of interstitial sites where guest ions can be inserted. Tungsten trioxide in its fully occupied state is transparent, but electrochemical reduction caused it to enter the EC state [13]. Much work on improving the performance of EC glass has been published. For example, Nagai et al. [14] published a study about the durability of the EC glazing. An all-solid-state structure can enhance the durability of EC glazing by reducing thermal effect. Reisfeld [15] published an EC glass fabrication technique involving mixing metal oxide from sol-gel using colloidal solutions of tungstic acid. The needed operational voltage was about ±1.3 V, and the number of cycles based on theoretical estimates was about 10^5~10^6 cycles. They noted that the rate of color change can be accelerated by increasing the conductivity of the tin-doped indium oxide (ITO) supporting glass. The blue coloration of the mixed valence tungsten in the EC film prevents the entry of solar light mainly in the UV and in a large part of the visible spectrum. They also mentioned that the effect of blocking solar radiation can be achieved by adding a fractional amount of MoO_3. Fang and Eames [16] pointed out the edge effect in EC windows. Even vacuum glazing small sizes (0.4 m × 0.4 m), leading to the thermal conductance in the central glazing region being 3.1% greater than the result, was calculated using an analytic model that does not consider edge effects. For larger sizes of vacuum glazing (1 m^2), the variation between the central glazing heat transmittance was calculated using finite volume and analytic models is 0.4%. Also, they mentioned that high temperatures will both damage the glazing system and make the indoor environment unbearable. The glass pane with the electrochromic layer must in all installations face the outdoor environment [17–21].

Transition metal oxides of WO_3 have transparent and semiconducting physical characteristics that make them usable for electrochromic film in electrochromic glass. In recent years WO_3 thin film has been manufactured by using an anodic oxidation process, purely using chemical solutions and parameters as objects of study [22, 23]. Nanoporous WO_3 thin film should be able to cause hydrogen (H^+) or lithium (Li^+) ions to be more rapid in the reaction process that carries on the proliferation, thereby increasing the color/bleach rate. Large-scale development of electrochromic glass based on porous films can potentially result in tremendous increase color/bleach rate, extended durability, insulated heat transfer, and energy savings. In addition, the production process will be relatively environmentally friendly. The knowledge generated by this research will significantly advance research in the area of the WO_3 film fabrication and use film as insulator and electrochromic film in electrochromic glass applications.

In principle, electrochemical impedance spectroscopy (EIS) measures a broad frequency range that can provide information on the interfaces of electron transport and charge transfer characteristics [24–29]. An analysis of electrochemical devices that describes electron transport and charge recombination in nanoparticle and nanotube film has been presented based on a transmission line model [30–33]. Kern et al. [34] indicated that Nyquist plot characteristics in the low-frequency range correspond to the electrolyte, while the middle-frequency range reflects the anode, and the high-frequency range corresponds to the cathode. Hoshikawa [35] also reported that the ω_1, ω_2, ω_3, and ω_4 semicircles were attributable to electron transfer at the transparent conduction oxide (TCO)/electron transport oxide (TiO_2) interface, TiO_2, TiO_2/electrolyte interface, and the diffusion impedance of ions in the electrolyte, respectively. Labidi et al. [36] discussed the EIS properties of surface morphology of WO_3 thin films which were prepared by RF sputtered, and, indicated that The AC impedance spectroscopy is a powerful method to understand the nature of conduction processes and the mechanism of gas/solid interactions. The Nyquist response

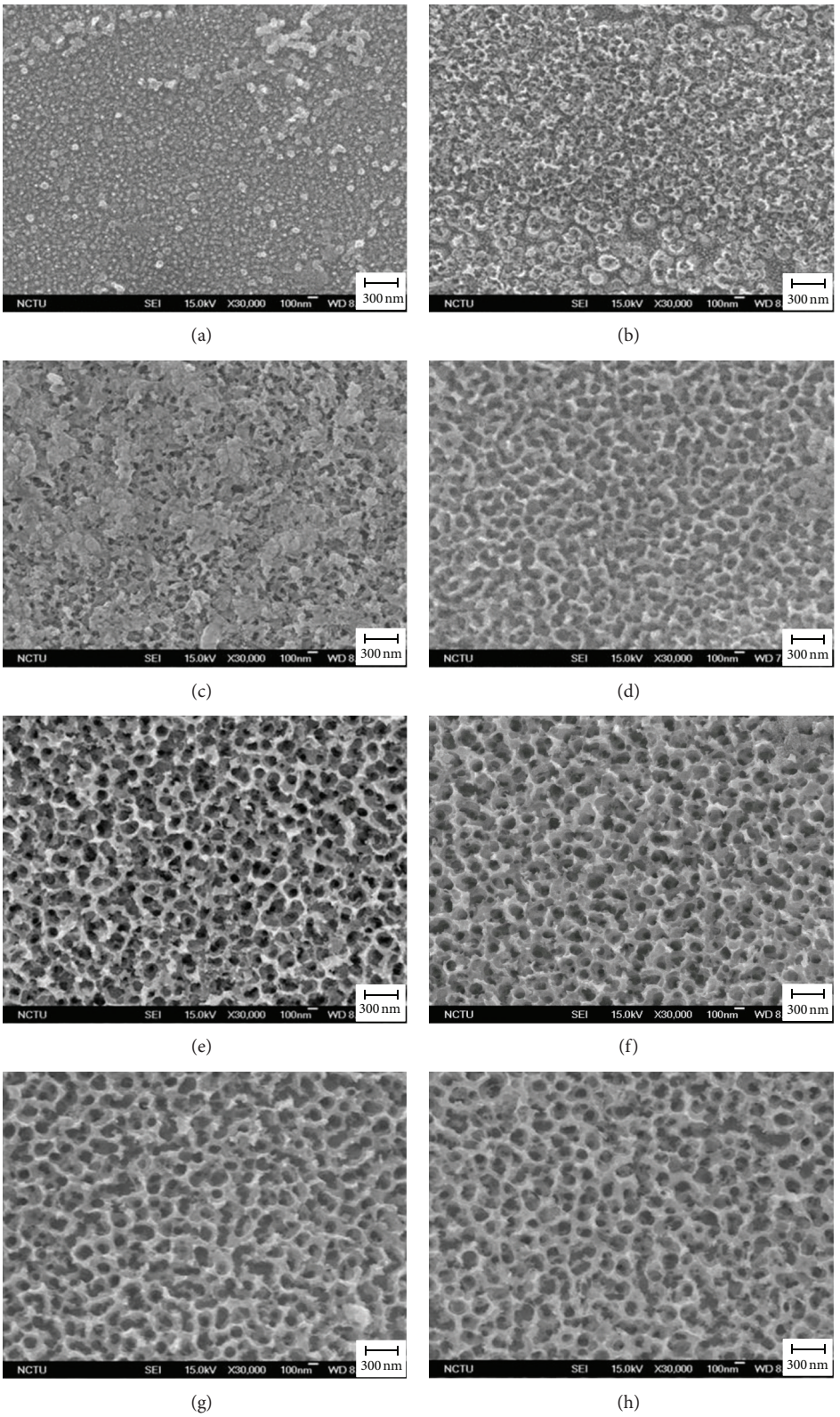

Figure 2: SEM images showing the porous structure on anodic tungsten oxide when tungsten was anodized in 0.4 wt.% NaF electrolyte, at 25°C for 1 hr and voltages of (a) 20 V, (b) 40 V, (c) 60 V, (d) 80 V, (e) 100 V, (f) 120 V, (g) 140 V, and (h) 160 V were applied.

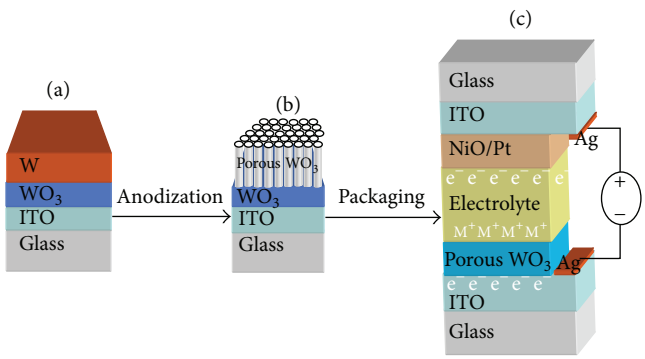

FIGURE 3: Schematic diagram of electrochromic glass based on porous WO_3 and multilayered structure. (a) An under layer of WO_3 was first deposited on the ITO glass and then a metal W film on the WO_3, (b) metal W film was used to form a porous WO_3 of electrochromic film by anodization, and (c) the 144 cm^2 electrochromic device includes a working electrode (ITO, WO_3), ion conductor (electrolyte), and counter (Pt, NiO_2, ITO).

dry air O_3 decomposed, and the adsorption of oxygen mainly affects the characteristics of the space charge region at the WO_3 grain boundaries.

Electrochromic glass has been developed since the 1970s and especially since the 1990s. However, there are still some aspects that could be improved such as the rate of color change and the lifetime of the EC glasses. In this paper, we use anodic porous WO_3 as EC film. We also report results from an EIS analysis that describes ohmic resistance, electron transfer resistance, diffusion resistance, charge-transfer resistance, contact capacitance, chemical capacitance, electrolysis capacitance, and double-layer capacitance in porous WO_3 EC glass.

2. Experimental Procedures

2.1. WO_3, W, NiO, *and* Pt *Films Deposition.* Porous WO_3 EC glass was fabricated on ITO glass as follows. (1) The WO_3 thin film was deposited by RF magnetron sputtering using a 4-inch tungsten metal target with a purity of 99.99%. A mixture of argon and oxygen gasses with an Ar/O_2 ratio of 3 was used for the deposition. Working pressure was set to 5×10^{-3} Torr and sputtering power during deposition was 100 W, while the thickness of the film was about 50 nm. (2) Tungsten (W) film was deposited by DC magnetron sputtering on WO_3. Working pressure (without O_2) was set to 5×10^{-3} Torr and sputtering power during deposition was 150 W, while the thickness of the film was about 100 nm. (3) NiO thin film was deposited by RF magnetron sputtering using a 4-inch nickel metal target with a purity of 99.99%. A mixture of argon and oxygen gasses with an Ar/O_2 ratio of 1 was used for the deposition. Working pressure was set to 5×10^{-3} Torr and sputtering power during deposition was 100 W, while the thickness of the film was about 50 nm. (4) Platinum (Pt) particles were deposited by DC magnetron sputtering on NiO. Working pressure (without O_2) was set to 5×10^{-3} Torr and sputtering power during deposition was 10 W for 14 sec.

2.2. Porous WO_3 *Fabrication.* The WO_3 porous film was made by anodization of tungsten film. According to the tungsten Porubaix diagram [37] when tungsten in an ionic containing electrolyte, for example, sodium fluoride (NaF) solution and applied a voltage, the tungsten (W) can oxidize to a porous tungsten oxide (WO_3). The specific surface area value of WO_3 can further be tested by BET (Brunauer, Emmett, Teller). Porous anodic tungsten oxide was fabricated by anodizing tungsten film in an anodization mold (Figure 1). A Ti counter-electrode net was fixed between a top cover and a middle cover, working tungsten film electrodes were fixed between the middle cover and a bottom cover, and the counter-working electrode distance was adjusted using a fixed column. At the same time, the working electrode and counter-electrode served, respectively, as the positive and negative terminal for a DC power supply. A sample of working and counter-electrodes was sandwiched in the mold, and a silicon rubber sheet was used to prevent electrolytic leaking into the mold. The top, middle, and bottom covers were fastened using threaded Teflon screws. Pressure was applied to the Teflon tubes to keep the top cover and bottom substrate in close contact. Finally, the working electrode in the mold was anodized in 0.4 wt.% NaF electrolyte, and voltage of 20 V to 160 V was applied for 1 h at 25°C. However, when the applied voltage is up to 160 V, the partial of porous WO_3 film was destroyed.

2.3. Electrochromic Device. Electrochromic devices with a configuration consisting of glass/ITO/WO_3/1 M $LiClO_4$-PC/Pt-NiO/ITO/glass and a size of 144 cm^2 were obtained by assembling two pieces of coated glass as follows. The two electrodes were assembled into a sandwich type cell and sealed with a hot-melt film (SX1170, Solaronix, thickness 0.1 mm) between electrodes interface. Electrolyte was injected into the space between the two electrodes with a syringe to fabricate an EC glass device. The device was then sealed with vacuum glue (Torr Seal) around electrodes and the electrolyte injecting hole.

2.4. Characterization of Electrochromic Glass. The micromorphology of the porous WO_3 film was examined using a scanning electron microscope (SEM, JEOL 6500). The optical transmission and reflection spectra were recorded using a UV-VIS-NIR optical photometer (JASCO V570) with an integrating sphere (JASCO ISN-470) in the range from 200 to 800 nm. The electrochromic properties were characterized using cyclic voltammetry (CV) method with a Zahner Impedance Measuring Unit (IM 6). Two electrodes were used to perform electrochemical tests in 1 M $LiClO_4$ electrolyte in propylene carbonate solution. The internal impedance was evaluated using electrochemical impedance spectroscopy (EIS). The EIS measurements were carried out with a Zahner Impedance Measuring Unit (IM 6). Electrochemical measurements were carried out using two electrode configurations: the glass/ITO/WO_3/porous WO_3 as working electrode and Pt-NiO/ITO electrode as counter-electrode. Cell impedance measurements were recorded over a frequency range of 3 M to 5 m Hz with AC amplitude of

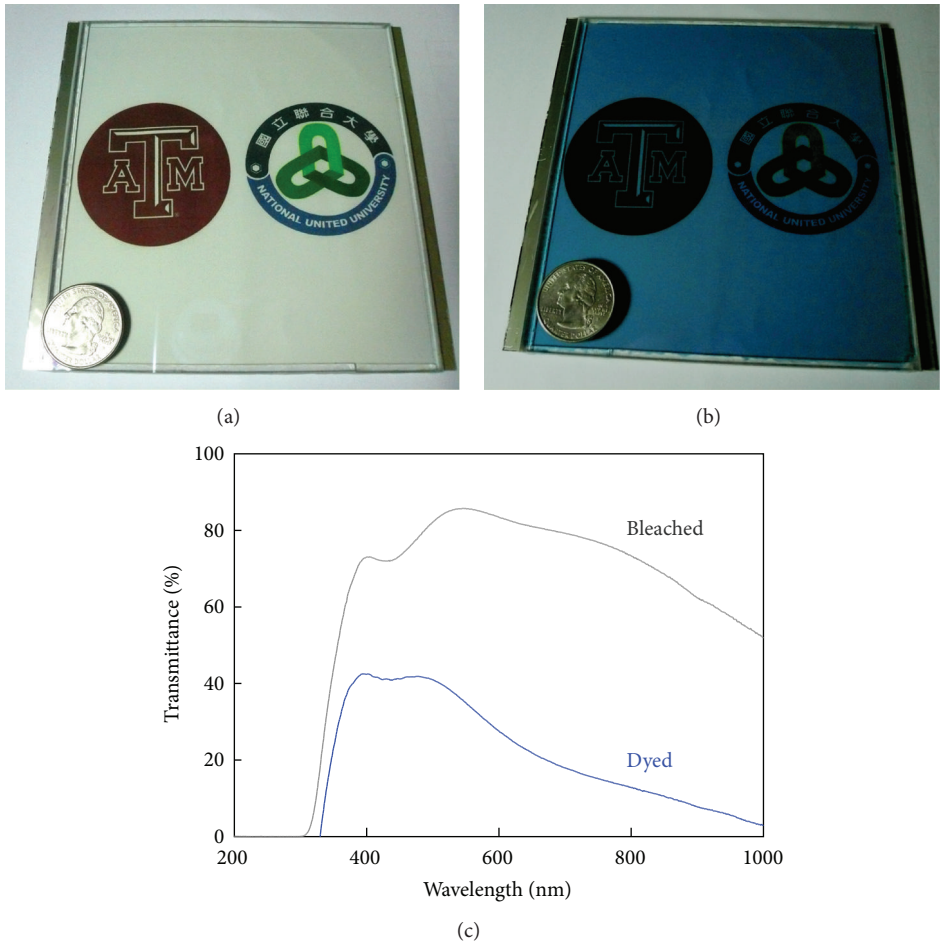

FIGURE 4: Images of electrochromic glass devices and optical transmittance spectrum: (a) electrochromic glass with transparent characteristics in a bleached state, (b) electrochromic glass with blue translucent characteristic in a dyed state, and (c) the glass has transparency of 82% and 21.1% in bleached and dyed states.

10 mV. The EIS data was analyzed by the equilibrium circuit mold and fitted by Microsoft Excel programs.

3. Results and Discussion

3.1. Structure and Characterization of EC Device. Figure 2 shows SEM images of the porous structure on the anodic tungsten oxide when tungsten was anodized in 0.4 wt.% NaF electrolyte at 25°C for 1 h and the following voltages were applied: (a) 20 V, (b) 40 V, (c) 60 V, (d) 80 V, (e) 100 V, (f) 120 V, (g) 140 V, and (h) 160 V. The WO_3 pore sizes increased with the amount of voltage applied. When 20 V was applied, the WO_3 film had an island structure but no pores formed. When voltage was increased to between 40 and 80 V, the WO_3 film was etched by fluorine ions (F^-) to form partially random porous WO_3 film. Furthermore, when voltages were increased to 100 V~160 V, the pores in the WO_3 widened to form a more regular porous WO_3 film.

Figure 3 shows a schematic diagram of EC glass using porous WO_3 and a multilayer structure. (a) An underlayer of WO_3 (50 nm) was first deposited on the ITO glass and then metal W film was deposited on the WO_3 (100 nm), (b) metal W film was used to form porous WO_3 electrochromic film by anodization, and (c) the 144 cm^2 electrochromic device including a working electrode (ITO (200 nm), WO_3), ion conductor (electrolyte), and counter (Pt, NiO (50 nm), ITO). Porous WO_3 is transparent before absorbing hydroxylated or lithiated materials. After voltage (−) is applied to WO_3 electrochromic film, its color changes to blue. WO_3 electrochromic film can serve as an intercalation host for H^+ and Li^+. Porous WO_3 film causes hydrogen (H^+) and lithium (Li^+) ions to be more rapid in the reaction process that carries on the proliferation, increasing the color/bleach rate. The reactions describing the intercalation/deintercalation of ionic species can be represented as

$$WO_3 + xH^+ + xe^- \Longleftrightarrow WO_{3-x}(OH)_x \quad (1)$$

$$WO_3 + xLi^+ + xe^- \Longleftrightarrow Li_xWO_3 \quad (2)$$

Figure 4 shows a photograph of the 144 cm^2 EC glass device. Figure 4(a) shows the as-prepared state and the transparent state. When a voltage is applied to the device, the active layer changes from transparent to the translucent

Table 1: Equilibrium circuits and mathematical results of real (Z_{RE}) and imaginary value (Z_{IM}) in porous WO_3 EC glass.

Equilibrium circuit	Z_{RE}	Z_{IM}
$R_0 + L_0$	R_0	ωL_0
$\{C_1//[R_1 + (C_2//R_2)]\}$	$\dfrac{[(R_2 + R_1) \times (1 - \omega^2 C_1 C_2 R_1 R_2) + (\omega C_2 R_1 R_2) \times (\omega C_2 R_2 + \omega C_1 R_2 + \omega C_1 R_1}{(1 - \omega^2 C_1 C_2 R_1 R_2)^2 + (\omega C_2 R_2 + \omega C_1 R_2 + \omega C_1 R_1)^2}$	$\dfrac{[(\omega C_2 R_1 R_2) \times (1 - \omega^2 C_1 C_2 R_1 R_2) - (R_2 + R_1) \times (\omega C_2 R_2 + \omega C_1 R_2 + \omega C_1 R_1)}{(1 - \omega^2 C_1 C_2 R_1 R_2)^2 + (\omega C_2 R_2 + \omega C_1 R_2 + \omega C_1 R_1)^2}$
$[C_3//(W + R_3)]$	$\dfrac{\sigma + R_3\sqrt{\omega}}{\sqrt{\omega} \times (1 + 2\sigma C_3\sqrt{\omega} + 2\sigma^2\omega C_3^2 + 2\sigma\omega^{1.5} C_3^2 R_3 + \omega^2 C_3^2 R_3^2)}$	$\dfrac{-\sigma - 2\sigma^2\sqrt{\omega}C_3 - 2\sigma\omega C_3 R_3 - \omega^{1.5} C_3 R_3^2}{\sqrt{\omega} \times (1 + 2\sigma C_3\sqrt{\omega} + 2\sigma^2\omega C_3^2 + 2\sigma\omega^{1.5} C_3^2 R_3 + \omega^2 C_3^2 R_3^2)}$
$(C_4//R_4)$	$\dfrac{R_4}{1 + (\omega R_4 C_4)^2}$	$\dfrac{-\omega R_4^2 C_4}{1 + (\omega R_4 C_4)^2}$
$(C_5//R_5)$	$\dfrac{R_5}{1 + (\omega R_5 C_5)^2}$	$\dfrac{-\omega R_5^2 C_5}{1 + (\omega R_5 C_5)^2}$

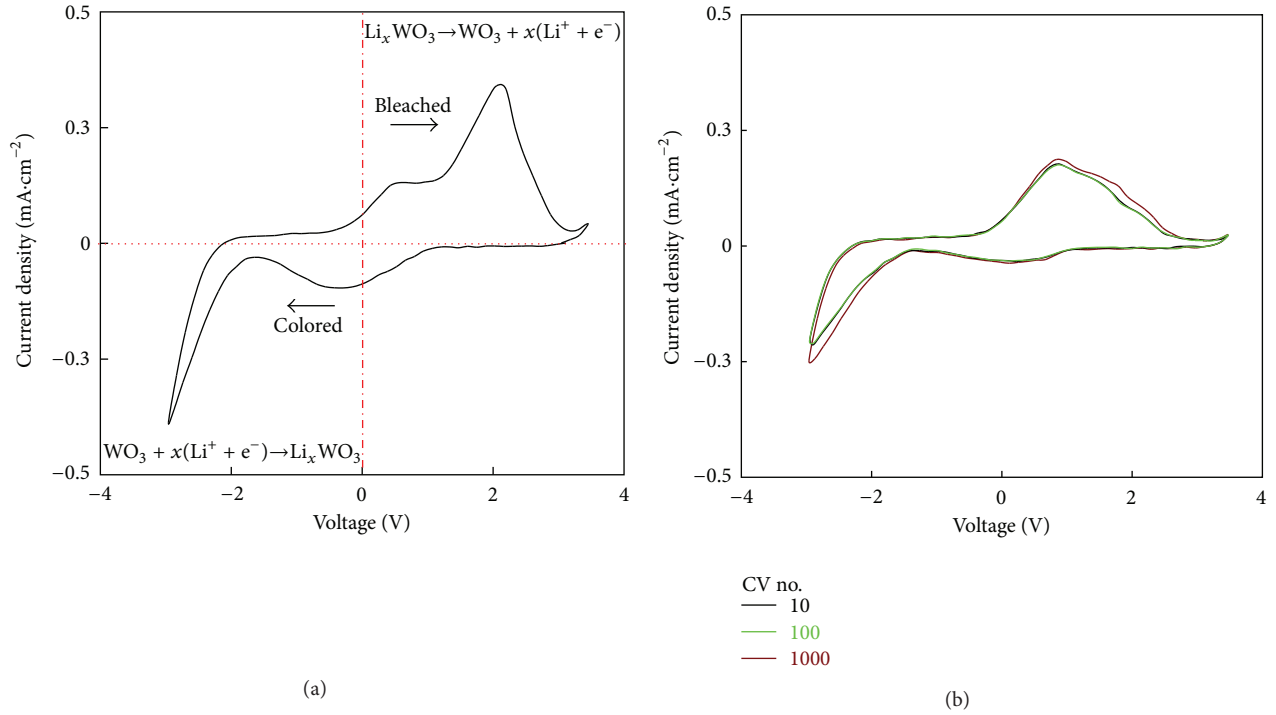

Figure 5: Cyclic voltammetry of porous WO_3 electrode performed between −3 V and +3 V with a scan rate of 50 mV in 0.1 M $HClO_4$-PC electrolyte: (a) 1 cycle and (b) 10, 100, and 1000 cycles.

Table 2: Parameters determined by fitting the EIS experimental data to the equivalent circuit shown in Figure 8.

Elements	Bleached	Dyed
R_0 (ohm)	6.29	6.25
R_1 (ohm)	1.2	1.1
R_2 (ohm)	0.5	0.65
R_3 (ohm)	110000	120000
R_4 (ohm)	1	1.7
R_5 (ohm)	7	45
C_1 (μF)	80	350
C_2 (μF)	900	420
C_3 (μF)	1200	3000
C_4 (μF)	1500	3800
C_5 (μF)	1100	2800

blue color associated with WO_3 reduction and simultaneous Li^+ insertion, as shown in Figure 4(b). Inversion of the applied voltage results in WO_3 oxidation and the device returns to its initial transparent state. The coloring voltage used in the EC glass was ±1.5 V over 30 sec. The optical transmittance characterization of the device in the wavelength range 400–800 nm is shown in Figure 4(c). The average transmittance in the visible region of the spectrum was above 75% in the bleached state and below 40% in the colored state, respectively. The cyclic voltammograms of porous WO_3 film are shown in Figure 5(a). The scan rate of measurements was 50 mV/s in the −4 V and +4 V ranges. It is known that electrochromic film is colored by charge injection ($WO_3 + x(Li^+ + e^-) \rightarrow Li_xWO_3$), and a part of this charge was extracted ($Li_xWO_3 \rightarrow WO_3 + x(Li^+ + e^-)$) during the subsequent bleaching process. Repeating the colored/bleached cycles, as shown in Figure 5(b), demonstrated good electrochemical stability as Li^+ ion can be almost inserted and extracted reversibly in the 10, 100, and 1000 cycle tests.

3.2. Internal Impedance Detection Using EIS Molding and Fitting. Figure 6(a) shows the EIS measured data of EC glass under dyed (■) and bleached (□) states. The Bode plot curves show that both bleached and dyed EC glasses have impedance values between 10^0 and 10^1 ohms in high-frequency ranges (from 10^2 to 10^6 Hz). Furthermore, they have impedance values between 10^1 and 10^5 ohms in low-frequency ranges (from 10^2 to 10^{-4} Hz). Because the working and counter-electrodes consist of ITO, Pt particles, and WO_3, and NiO semiconductor films, the electrodes have low impedance. On the other hand, the electrolyte is composed of 1 M $LiClO_4$ in propylene carbonate, which has high impedance. Therefore, the impedance in high- and low- frequency ranges is represented by the electrodes and electrolyte characterizations in the Bode plot. The Nyquist plots also show that the EC glass had higher impedance in a bleached state than in a dyed state in wide frequency ranges, as shown in Figure 6(b), and in high- frequency ranges, as shown in Figure 6(c).

An EC glass circuit, shown in Figure 7(a), was constructed based on the EC glass structure. In this circuit, the ohmic impedance includes ITO resistance (R_{01}, R_{03}) and transport wire resistance (R_{02}). The working parts

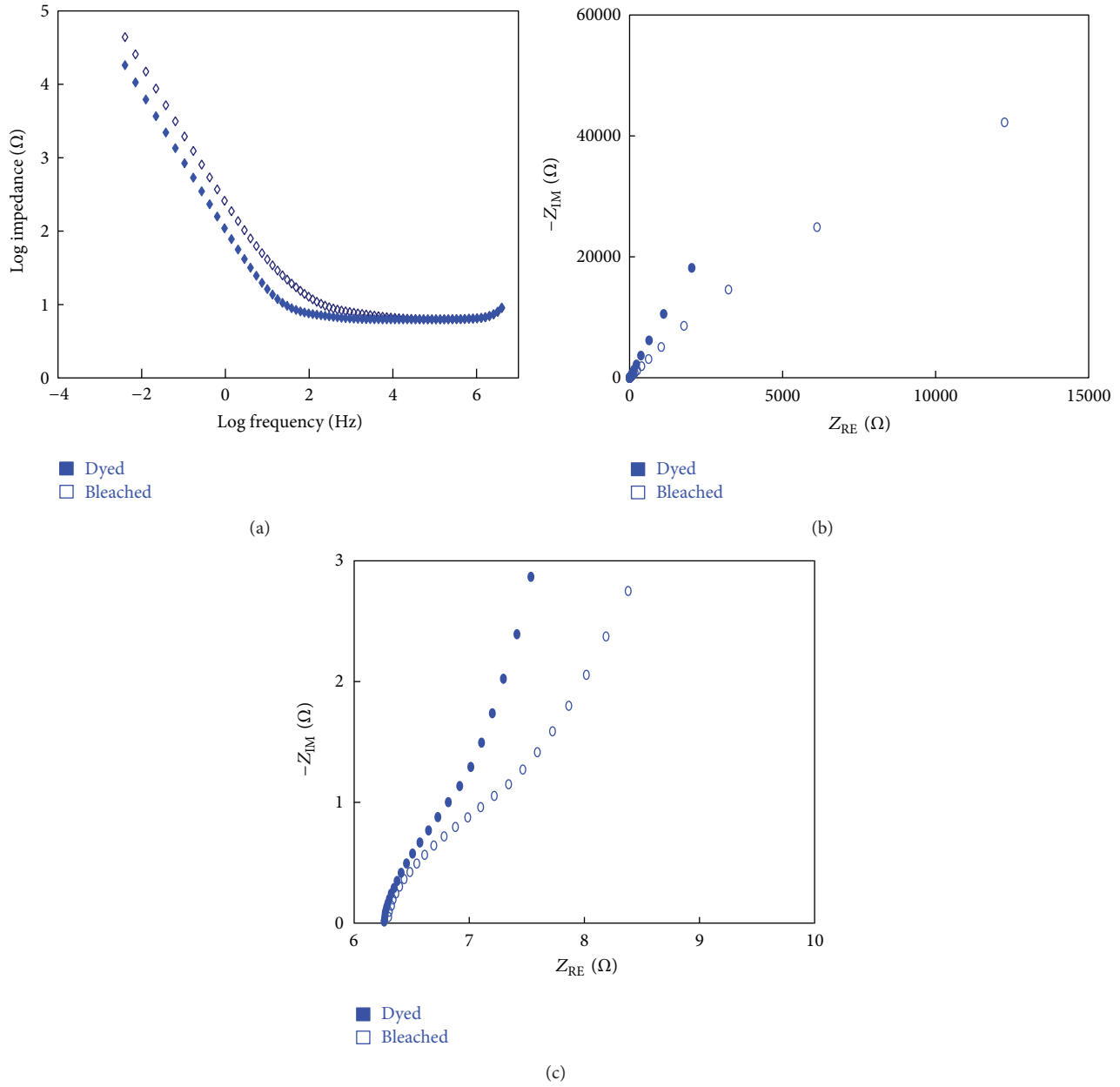

FIGURE 6: AC impedance curves of porous WO_3 electrode from electrochromic glass under dyed (■) and bleached (□) states: (a) bode plot, (b) Nyquist plot, and (c) Nyquist plot in a high-frequency range.

of the ITO/WO_3 and WO_3/electrolyte interfaces are presented as $C_1//R_1$ and $C_2//R_2$. The electrolyte is presented as $C_3/(R_3 + W)$. The counterparts of the NiO/electrolyte and ITO/NiO interfaces are presented as $C_4//R_4$ and $C_5//R_5$. The equilibrium circuit, including a series circuit of working electrode, electrolyte, and counter electrode are shown in Figure 7(b). In order to present semicircles and simplify the mathematical operations analysis in each working, electrolyte, and counterpart, the equivalent circuit is portrayed separately in Figure 7(c). Figure 8 shows the experimental (O) and fitted (—) data for the EG glass impedance under (a) dyed and (b) bleached conditions; the inset figures are the Nyquist plots in high-frequency ranges. Figure 9 shows the equilibrium circuit and simulation plot of EG glass (a) working ($C_1//R_1$+($C_2//R_2$)), (b) electrolyte ($C_3//(R_3 + W)$, (c) electrolyte/counter ($C_4//R_4$), and (d) counter ($C_4//R_4$) impedances in the bleached state. Also, (e), (f), (g), and (h) show the EG glass impedances in the dyed state. The detail equilibrium circuits and mathematical results were in Table 1 and the appendix.

Based on the equilibrium circuit model in Figure 7, the EIS data in Figure 8, and the speared circuit model in Figure 9, the fitted results are in Table 2. The ohmic resistance (R_0) is independent of dyed/bleached states. The values of R_0 (6.25 to 6.29 Ω) can be observed at the start point on the Nyquist plot. The resistance between ITO and WO_3 is called the contact

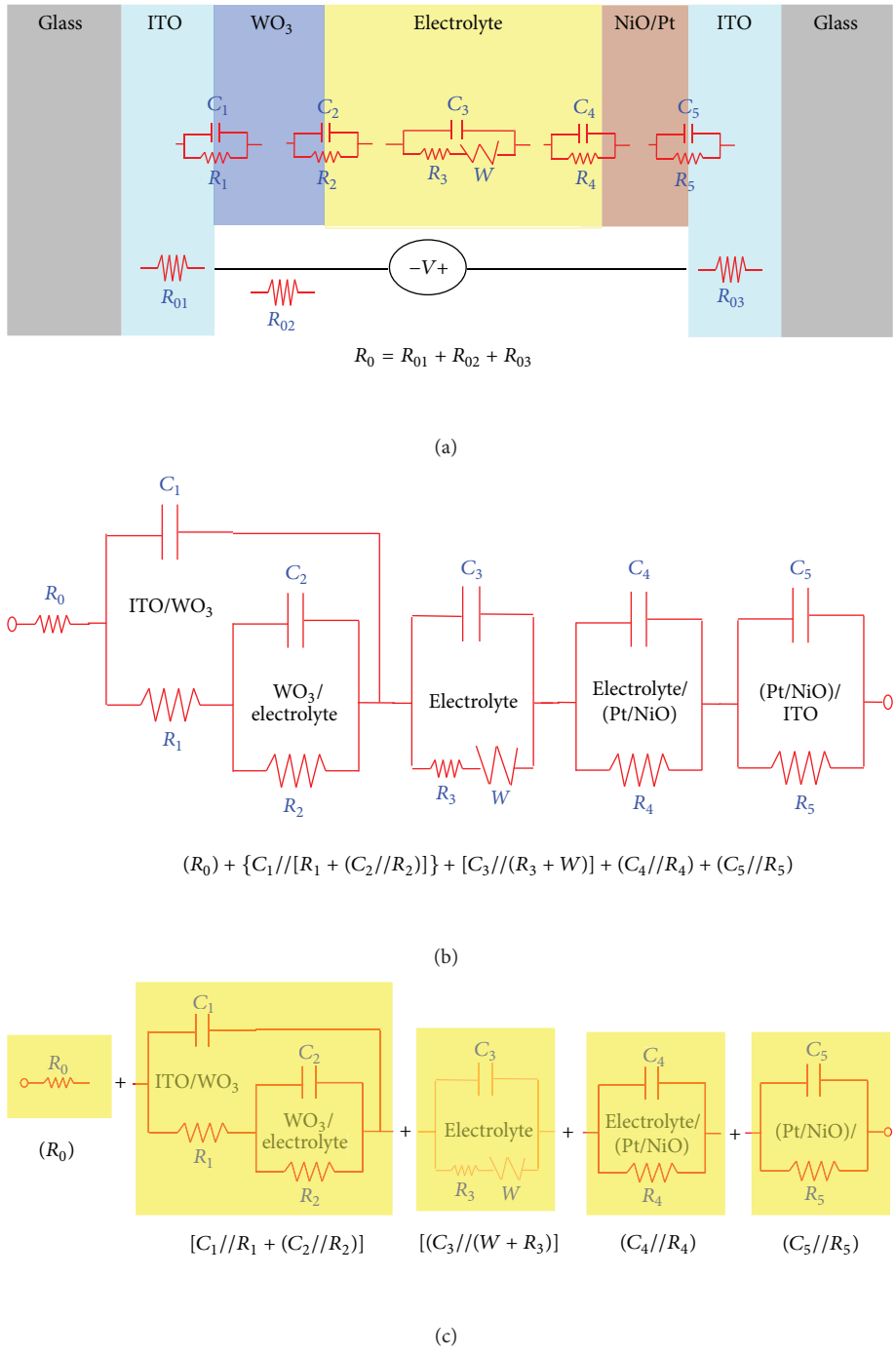

FIGURE 7: Schematic diagram of (a) porous WO_3 EC glass structure that can be simulated by using resister, capacitor, and Warburg impedance. Each interface of ITO/WO_3, WO_3/electrolyte, electrolyte/NiO, and NiO/ITO can be simulated using a RC parallel circuit, and bulk material such as ITO and conducting wire can be simulated by a series of resistors. (b) and (c) Equivalent circuit used for modeling the EIS of EC glass. The impedance of the bulk matter is simulated by $R_0 = R_{01} + R_{02} + R_{03}$, the impedance of working electrode is simulated by $(C_1//R_1 + (C_2//R_2))$, the electrolyte is simulated by $C_3//(R_3 + W)$, and the counter electrode is simulated by $(C_4//R_4) + (C_5//R_5)$.

resistance (R_1). Lower R_1 (1.2 and 1.1 Ω) was observed in the presence of a good contact between the ITO and WO_3. The other resistances–electron transfer resistance (R_2), diffusion resistance (R_3), charge-transfer resistance (R_4), and contact resistance (R_5)–reflect the working, electrolyte, and counter resistances. When the EC glass is dyed, the Li^+ and H^+ ions dope to WO_3 film and the concentrations of Li^+ and H^+ ions in the electrolyte are reduced. Therefore, the electrodes/electrolyte and bulk electrolyte interfaces of R_2, R_4, and R_3 have higher resistances in the dyed (0.65, 1.7, and

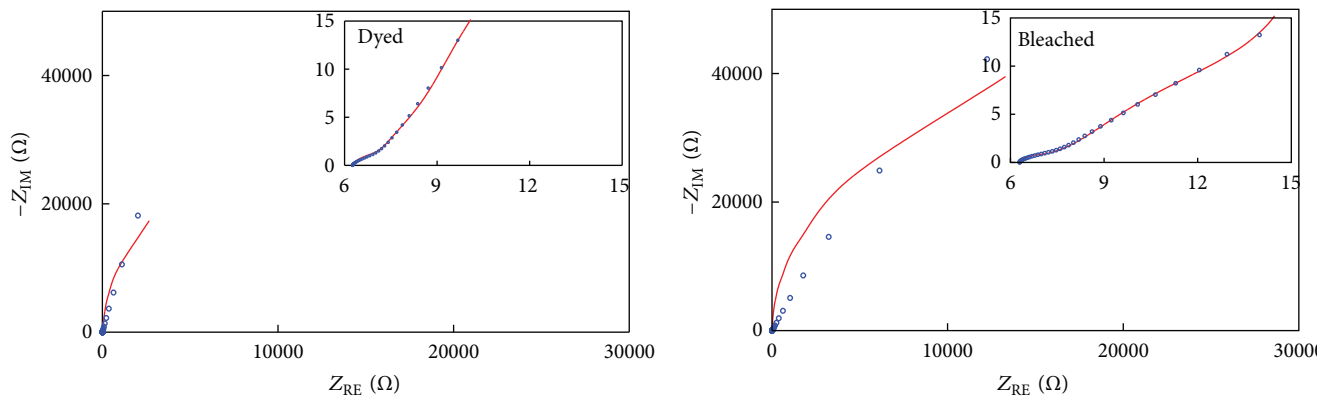

(a) (b)

FIGURE 8: Experimental (○) and fitted (—) data for EC glass under (a) dyed and (b) bleached states; inset figures are Nyquist plots in high frequency ranges.

120000 Ω) than in the bleached (0.5, 1.0, and 110000 Ω) state. In contrast, when Li^+ ions move back to the electrolyte and dope to NiO film, R_5 has higher resistance in bleached (45 Ω) than in dyed (7 Ω) states.

The capacitance reflects the characteristic of charge quantity on matter interface. Since a resistance and capacitor parallel ($R//C$) circuit can present a semicircle on a Nyquist plot, expressed mathematically, the imaginary value is $[\omega R^2 C/(1 + (\omega RC)^2)]$, where ω is angular frequency, R is resistance, and C is capacitor. When $1 + (\omega RC)^2$ tends to zero, the imaginary has a larger value; therefore the highest point on the semicircle can be evaluated as $\omega = 1/RC$. There are clear semicircles of electrolysis impedance shown in the simulation results in Figure 9, except in Figures 9(b) and 9(c). Because the resistances refer to the length of the diameter of the semicircle, the electrolysis capacitances can be calculated by $C = 1/\omega_{peak}R$, where ω_{peak} is the angular frequency at the top of the semicircle.

The contact capacitance (C_1) reflects the charge transfer between the ITO and WO_3 interface. Charges (Li^+) transferring from WO_3 to ITO in EC glass have a higher C_1 in the colored (350 μF) than that in the bleached (80 μF) state. The chemical capacitance (C_2) reflects the charges in the WO_3 and electrolyte interface. EC glass has a lower C_2 in the colored (900 μF) than in the bleached (420 μF) state. When EC glass is bleached, most of the charges move back to the bulk electrolyte and there is a greater quantity of charges on the WO_3/electrolyte interface than that in the colored state. Because the electrolyte (1 M $LiClO_4$+PC) used in the EC glass has low conductivity, a Warburg impedance characteristic can be observed in Nyquist plot. A Warburg impedance element can be used to model semi-infinite linear diffusion. The equilibrium circuit of a low conductivity electrolyte includes a capacitor (C_3) series to parallel elements ($R_3//W$) where W is Warburg impedance ($2\sigma^2/j\omega$; σ is Warburg constant. The electrolyte capacitance (C_3) reflects the capacitance effect in electrolyte. Because charges move back to the electrolyte, the EC glass has a lower C_3 in the colored (1200 μF) than in the bleached (3000 μF) state.

The double-layer capacitance (C_4) reflects the electrolyte/counter interface and also reflects the surface area of Pt on the NiO. It is expected that Pt sputter deposition on the counter electrode increases the surface area of the counter and, consequently, promotes the separated $LiClO_4$ into Li^+ and ClO_4^-. Because ClO_4^- moves to the counter surface in the colored state, the EC glass has a higher C_4 in the colored (3800 μF) than in the bleached (1500 μF) state. The contact capacitance (C_5) reflects charge transfer at the ITO and NiO interface. Because charges (ClO_4^-) transfer from NiO to ITO, the EC glass has a higher C_5 in the colored (2800 μF) than in the bleached (1100 μF) state.

The impedance spectra of the porous WO_3 EC glass showed internal resistance consisting of at least thirteen components. It was found that the resistances of the ITO (R_{01} and R_{03}) and the transport wire (R_{02}) appeared as ohmic impedance. The ohmic impedance value was not affected by colored/bleached states. The other resistances—electron transfer resistance (R_1, R_2, and R_5), diffusion resistance (R_3), and charge-transfer resistance (R_4)—as the internal resistances were affected by colored/bleached states that are determinative in the performance of EC glass. The interface capacitances of contact capacitance (C_1 and C_5), chemical capacitance (C_2), electrolysis capacitance (C_3), and double-layer capacitance (C_4) are determinative in the performance of charges on the interfaces.

4. Conclusions

A 144 cm^2 electrochromic device was fabricated using ITOs, NiO, porous WO_3 film, and Pt particles. The characteristics of the EC glass were determined using UV-VIS-NIR, CV, and EIS equipments. The average transmittance in the colored and bleached states was 15.7% and 60.2%, respectively. The repeatability of the colored/bleached cycles over 1000 cyclic voltammograms tests was good. In EIS analysis, the

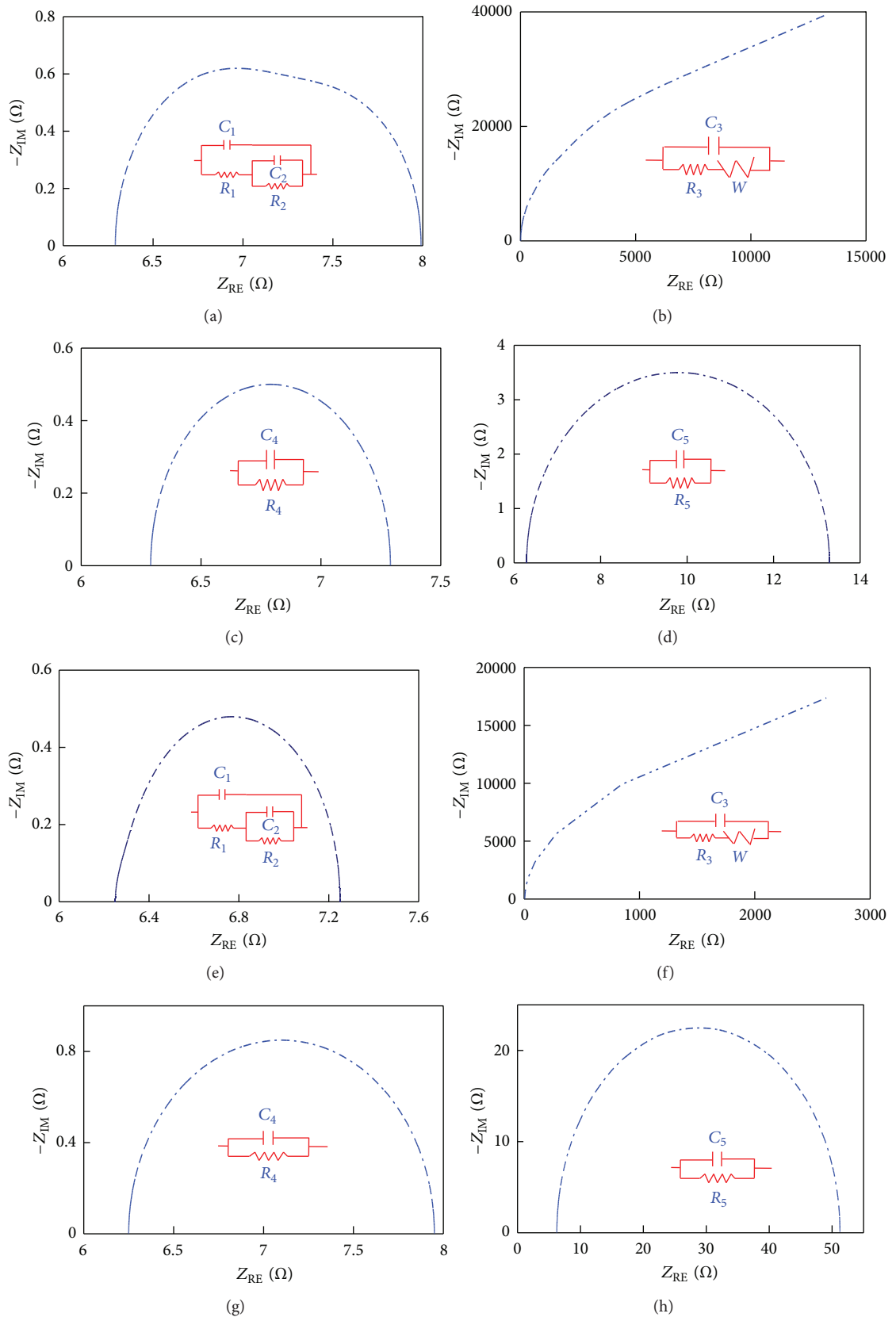

FIGURE 9: Nyquist plots and simulated circuits in EC glass of working electrode (a, e), electrolyte (b, f), and counter electrode (c, d, g, h) under dyed (a, b, c, d) and bleached (e, f, g, h) states.

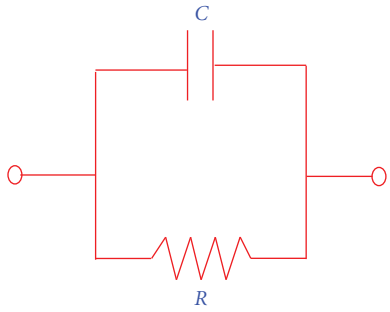

Figure 10

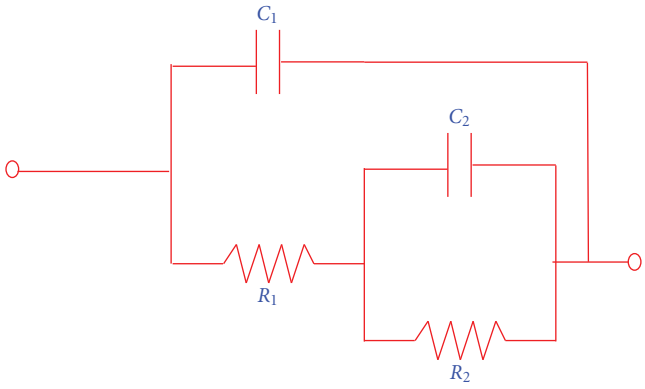

Figure 11

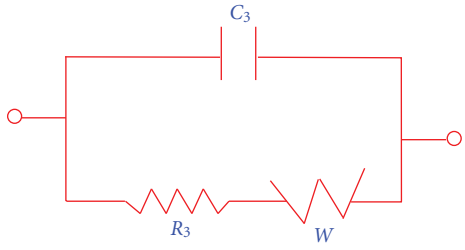

Figure 12

ohmic impedance (R_0) value was about 6.3 Ω. The other resistances—electrodes/electrolyte and electrolyte interfaces (R_2, R_4, and R_3)—have higher resistances in colored (Li^+ ions move to WO_3) than in bleached (Li^+ ions move back to electrolyte and NiO) states. In contrast, R_5 has higher resistance in the bleached than in the dyed state. The contact capacitance (C_1 and C_5), electrolysis capacitance (C_3), and double-layer capacitance (C_4) all have higher values in the colored than in the bleached state, but the chemical capacitance (C_2) is the opposite.

We have shown that anodic WO_3 can be used as electrochromic film in EC glass. The fabrication process can be extended to TiO_2 and Ta_2O_5, which are electrochromic and solid charge conductive films. A detailed study of porous films used for EC glass using anodization will be described in a future paper.

Appendix

(1) $(C//R)$. See also Figure 10

$$\begin{aligned}\frac{Z_C R}{Z_C + R} &= \frac{R/j\omega C}{(1/j\omega C) + R}\\ &= \frac{R}{1 + j\omega RC} = \frac{R(1 - j\omega RC)}{1 + (\omega RC)^2}\\ &= \frac{R}{1 + (\omega RC)^2} + j\frac{-\omega R^2 C}{1 + (\omega RC)^2}\end{aligned} \tag{A.1}$$

$$Z_{\mathrm{RE}} = \frac{R}{1 + (\omega RC)^2}$$

$$Z_{\mathrm{IM}} = \frac{-\omega R^2 C}{1 + (\omega RC)^2}.$$

(2) $\{C_1//[R_1 + (C_2//R_2)]\}$. See also Figure 11

$$\begin{aligned}&\left(\frac{Z_1 Z_2 R_2 + Z_1 R_1 Z_2 + Z_1 R_1 R_2}{Z_2 + R_2}\right)\\ &\quad\times\left(\frac{Z_2 R_2 + R_1 Z_2 + R_1 R_2 + Z_1 Z_2 + Z_1 R_2}{Z_2 + R_2}\right)^{-1}\\ &= \left(\frac{R_2}{j^2\omega^2 C_1 C_2} + \frac{R_1}{j^2\omega^2 C_1 C_2} + \frac{R_1 R_2}{j\omega C_1}\right)\\ &\quad\times\left(\frac{R_2}{j\omega C_2} + \frac{R_1}{j\omega C_2} + R_1 R_2\right.\\ &\qquad\left. + \frac{1}{j^2\omega^2 C_1 C_2} + \frac{R_2}{j\omega C_1}\right)^{-1}\\ &= \left(\frac{R_2 + R_1 + j\omega C_2 R_1 R_2}{j^2\omega^2 C_1 C_2}\right)\\ &\quad\times\left(\left(j\omega C_1 R_2 + j\omega C_1 R_1 + j^2\omega^2 C_1 C_2 R_1 R_2 + 1\right.\right.\\ &\qquad\left.\left. + j\omega C_2 R_2\right)\times\left(j^2\omega^2 C_1 C_2\right)^{-1}\right)^{-1}\\ &= \left(R_2 + R_1 + j\omega C_2 R_1 R_2\right)\\ &\quad\times\left(\left(1 - \omega^2 C_1 C_2 R_1 R_2\right)\right.\\ &\qquad\left. + j\left(\omega C_2 R_2 + \omega C_1 R_2 + \omega C_1 R_1\right)\right)^{-1}\\ &= \left(\left(R_2 + R_1 + j\omega C_2 R_1 R_2\right)\right.\\ &\quad\times\left[\left(1 - \omega^2 C_1 C_2 R_1 R_2\right)\right.\\ &\qquad\left.\left. - j\left(\omega C_2 R_2 + \omega C_1 R_2 + \omega C_1 R_1\right)\right]\right)\\ &\quad\times\left(\left(1 - \omega^2 C_1 C_2 R_1 R_2\right)^2\right.\\ &\qquad\left. + \left(\omega C_2 R_2 + \omega C_1 R_2 + \omega C_1 R_1\right)^2\right)^{-1}\end{aligned}$$

$$
\begin{aligned}
&= \left(\left[(R_2 + R_1) + (j\omega C_2 R_1 R_2) \right] \right. \\
&\quad \times \left[\left(1 - \omega^2 C_1 C_2 R_1 R_2\right) \right. \\
&\qquad \left. \left. -j\left(\omega C_2 R_2 + \omega C_1 R_2 + \omega C_1 R_1\right) \right] \right) \\
&\quad \times \left(\left(1 - \omega^2 C_1 C_2 R_1 R_2\right)^2 \right. \\
&\qquad \left. + \left(\omega C_2 R_2 + \omega C_1 R_2 + \omega C_1 R_1\right)^2 \right)^{-1} \\
&= \left(\left[(R_2 + R_1) \times \left(1 - \omega^2 C_1 C_2 R_1 R_2\right) \right. \right. \\
&\quad \left. \left. + (\omega C_2 R_1 R_2) \times (\omega C_2 R_2 + \omega C_1 R_2 + \omega C_1 R_1) \right] \right) \\
&\qquad \times \left(\left(1 - \omega^2 C_1 C_2 R_1 R_2\right)^2 \right. \\
&\qquad \left. + \left(\omega C_2 R_2 + \omega C_1 R_2 + \omega C_1 R_1\right)^2 \right)^{-1} \\
&\quad + \left(j \left[-(R_2 + R_1) \times \left(\omega C_2 R_2 + \omega C_1 R_2 + \omega C_1 R_1\right) \right. \right. \\
&\qquad \left. \left. + (\omega C_2 R_1 R_2) \times \left(1 - \omega^2 C_1 C_2 R_1 R_2\right) \right] \right) \\
&\qquad \times \left(\left(1 - \omega^2 C_1 C_2 R_1 R_2\right)^2 \right. \\
&\qquad \left. + \left(\omega C_2 R_2 + \omega C_1 R_2 + \omega C_1 R_1\right)^2 \right)^{-1} \\
Z_{\mathrm{RE}} &= \left(\left[(R_2 + R_1) \times \left(1 - \omega^2 C_1 C_2 R_1 R_2\right) + (\omega C_2 R_1 R_2) \right. \right. \\
&\qquad \left. \left. \times (\omega C_2 R_2 + \omega C_1 R_2 + \omega C_1 R_1) \right] \right) \\
&\qquad \times \left(\left(1 - \omega^2 C_1 C_2 R_1 R_2\right)^2 \right. \\
&\qquad \left. + \left(\omega C_2 R_2 + \omega C_1 R_2 + \omega C_1 R_1\right)^2 \right)^{-1} \\
Z_{IM} &= \left(\left[(\omega C_2 R_1 R_2) \times \left(1 - \omega^2 C_1 C_2 R_1 R_2\right) \right. \right. \\
&\qquad \left. \left. - (R_2 + R_1) \times (\omega C_2 R_2 + \omega C_1 R_2 + \omega C_1 R_1) \right] \right) \\
&\qquad \times \left(\left(1 - \omega^2 C_1 C_2 R_1 R_2\right)^2 \right. \\
&\qquad \left. + \left(\omega C_2 R_2 + \omega C_1 R_2 + \omega C_1 R_1\right)^2 \right)^{-1}.
\end{aligned}
\tag{A.2}
$$

(3) $[C_3//(W + R_3)]$. See also Figure 12

$$
\begin{aligned}
&\left(\frac{1}{j\omega C_3} \times \left(R_3 + \frac{2\sigma^2}{j\omega} \right) \right) \\
&\quad \times \left(\frac{1}{j\omega C_3} + \left(R_3 + \frac{2\sigma^2}{j\omega} \right) \right)^{-1} \\
&= \left(\frac{1}{j\omega C_3} \times \frac{j\omega R_3 + 2\sigma^2}{j\omega} \right) \\
&\quad \times \left(\frac{1}{j\omega C_3} + \frac{j\omega R_3 + 2\sigma^2}{j\omega} \right)^{-1} \\
&= \left(\frac{j\omega R_3 + 2\sigma^2}{\omega^2 C_3} \right) \\
&\quad \times \left(\frac{j\omega - \omega^2 C_3 R_3 + 2j\omega C_3 \sigma^2}{\omega^2 C_3} \right)^{-1} \\
&= -\left(\left(j\omega R_3 + 2\sigma^2 \right) \times \left[\omega^2 C_3 R_3 + j\left(\omega + 2\omega C_3 \sigma^2\right) \right] \right) \\
&\qquad \times \left(\left[\omega^2 C_3 R_3 - j\left(\omega + 2\omega C_3 \sigma^2\right) \right] \right. \\
&\qquad \left. \times \left[\omega^2 C_3 R_3 + j\left(\omega + 2\omega C_3 \sigma^2\right) \right] \right)^{-1} \\
&= -\left(j\omega^3 R_3^2 C_3 - \omega^2 R_3 + j2\omega^2 R_3 C_3 \sigma^2 \right. \\
&\qquad \left. + 2\sigma^2 \omega^2 C_3 R_3 + j2\omega\sigma^2 + j4\omega C_3 \sigma^4 \right) \\
&\qquad \times \left(\omega^4 C_3^2 R_3^2 + \omega^2 + 4\omega^2 C_3^2 \sigma^4 + 4\omega^2 C_3 \sigma^2 \right)^{-1} \\
Z_{\mathrm{RE}} &= \frac{\omega^2 R_3 - 2\sigma^2 \omega^2 C_3 R_3}{\omega^4 C_3^2 R_3^2 + \omega^2 + 4\omega^2 C_3^2 \sigma^4 + 4\omega^2 C_3 \sigma^2} \\
Z_{\mathrm{IM}} &= -\frac{\omega^3 R_3^2 C_3 + 2\omega^2 R_3 C_3 \sigma^2 + 2\omega\sigma^2 + 4\omega C_3 \sigma^4}{\omega^4 C_3^2 R_3^2 + \omega^2 + 4\omega^2 C_3^2 \sigma^4 + 4\omega^2 C_3 \sigma^2}.
\end{aligned}
\tag{A.3}
$$

Acknowledgment

The authors gratefully appreciate the financial support of the National Science Council of ROC under the contract no. (101-2627-M-239-001-).

References

[1] Y. Djaoued, S. Balaji, and R. Brüning, "Electrochromic devices based on porous tungsten oxide thin films," *Journal of Nanomaterials*, vol. 2012, Article ID 674168, 9 pages, 2012.

[2] N. N. Dinh, D. H. Ninh, T. T. Thao, and T. V. Van, "Mixed nanostructured Ti-W oxides films for efficient electrochromic windows," *Journal of Nanomaterials*, vol. 2012, Article ID 781236, 7 pages, 2012.

[3] G. B. Smith, S. Dligatch, R. Sullivan, and M. G. Hutchins, "Thin film angular selective glazing," *Solar Energy*, vol. 62, no. 3, pp. 229–244, 1998.

[4] J. Mohelnikova, "Materials for reflective coatings of window glass applications," *Construction and Building Materials*, vol. 23, no. 5, pp. 1993–1998, 2009.

[5] NREL, http://www.nrel.gov/ .

[6] X. Sun, Z. Liu, and H. Cao, "Effects of film density on electrochromic tungsten oxide thin films deposited by reactive dc-pulsed magnetron sputtering," *Journal of Alloys and Compounds*, vol. 504, no. 1, pp. S418–S421, 2010.

[7] P. M. Kadam, N. L. Tarwal, P. S. Shinde et al., "Enhanced optical modulation due to SPR in gold nanoparticles embedded WO_3 thin films," *Journal of Alloys and Compounds*, vol. 509, no. 5, pp. 1729–1733, 2011.

[8] C. M. Lampert, "Heat mirror coatings for energy conserving windows," *Solar Energy Materials*, vol. 6, no. 1, pp. 1–41, 1981.

[9] R. E. Collins and T. M. Simko, "Current status of the science and technology of vacuum glazing," *Solar Energy*, vol. 62, no. 3, pp. 189–213, 1998.

[10] T. S. Eriksson, C. G. Granqvist, and J. Karlsson, "Transparent thermal insulation with infrared-absorbing gases," *Solar Energy Materials*, vol. 16, no. 1–3, pp. 243–253, 1987.

[11] H. Byker, in *Proceedings of the Symposium on Electrochromic Materials II*, K. C. Ho and D. A. MacArthur, Eds., vol. PV 94-2 of *Electrochemical Society Proceeding Series*, Pennington, NJ, USA, 1994.

[12] S. Supothina, P. Seeharaj, S. Yoriya, and M. Sriyudthsak, "Synthesis of tungsten oxide nanoparticles by acid precipitation method," *Ceramics International*, vol. 33, no. 6, pp. 931–936, 2007.

[13] P. R. Somani and S. Radhakrishnan, "Electrochromic materials and devices: present and future," *Materials Chemistry and Physics*, vol. 77, no. 1, pp. 117–133, 2003.

[14] J. Nagai, G. D. McMeeking, and Y. Saitoh, "Durability of electrochromic glazing," *Solar Energy Materials and Solar Cells*, vol. 56, no. 3-4, pp. 309–319, 1999.

[15] R. Reisfeld, M. Zayat, H. Minti, and A. Zastrow, "Electrochromic glasses prepared by the sol-gel method," *Solar Energy Materials and Solar Cells*, vol. 54, no. 1–4, pp. 109–120, 1998.

[16] Y. Fang and P. C. Eames, "The effect of glass coating emittance and frame rebate on heat transfer through vacuum and electrochromic vacuum glazed windows," *Solar Energy Materials and Solar Cells*, vol. 90, no. 16, pp. 2683–2695, 2006.

[17] Y. C. Nah, A. Ghicov, D. Kim, S. Berger, and P. Schmuki, "TiO_2-WO_3 composite nanotubes by alloy anodization: growth and enhanced electrochromic properties," *Journal of the American Chemical Society*, vol. 130, no. 48, pp. 16154–16155, 2008.

[18] A. B. Powell, C. W. Bielawski, and A. H. Cowley, "Design, synthesis, and study of main chain poly(N-heterocyclic carbene) complexes: applications in electrochromic devices," *Journal of the American Chemical Society*, vol. 132, no. 29, pp. 10184–10194, 2010.

[19] M. S. Burdis and D. G. Weir, Sage Electrochromics, Electrochromic devices and methods, Patent US 2006/0209383A1, 2006.

[20] S. S. Kalagi, D. S. Dalavi, R. C. Pawar, N. L. Tarwal, S. S. Mali, and P. S. Patil, "Polymer assisted deposition of electrochromic tungsten oxide thin films," *Journal of Alloys and Compounds*, vol. 493, no. 1-2, pp. 335–339, 2010.

[21] C. Santato, M. Odziemkowski, M. Ulmann, and J. Augustynski, "Crystallographically oriented mesoporous WO_3 films: synthesis, characterization, and applications," *Journal of the American Chemical Society*, vol. 123, no. 43, pp. 10639–10649, 2001.

[22] C. Cai, D. Guan, and Y. Wang, "Solution processing of V_2O_5-WO_3 composite films for enhanced Li-ion intercalation properties," *Journal of Alloys and Compounds*, vol. 509, no. 3, pp. 909–915, 2010.

[23] V. Karastoyanov and M. Bojinov, "Anodic oxidation of tungsten in sulphuric acid solution-Influence of hydrofluoric acid addition," *Materials Chemistry and Physics*, vol. 112, no. 2, pp. 702–710, 2008.

[24] G. Kron, T. Egerter, J. H. Werner, and U. Rau, "Electronic transport in dye-sensitized nanoporous TiO_2 solar cells-Comparison of electrolyte and solid-state devices," *Journal of Physical Chemistry B*, vol. 107, no. 15, pp. 3556–3564, 2003.

[25] K. Schwarzburg and F. Willig, "Diffusion impedance and space charge capacitance in the nanoporous dye-sensitized electrochemical solar cell," *Journal of Physical Chemistry B*, vol. 107, no. 15, pp. 3552–3555, 2003.

[26] G. He, L. Zhao, Z. Zheng, and F. Lu, "Determination of electron diffusion coefficient and lifetime in dye-sensitized solar cells by electrochemical impedance spectroscopy at high fermi level conditions," *Journal of Physical Chemistry C*, vol. 112, no. 48, pp. 18730–18733, 2008.

[27] C. C. Chen, D. Fang, and Z. Luo, "Fabrication and characterization of highly-ordered valve-metal oxide nanotubes and their derivative nanostructures: a review," *Reviews in Nanoscience and Nanotechnology*, vol. 1, no. 4, pp. 229–256, 2012.

[28] S. R. Biaggio, R. C. Rocha-Filho, J. R. Vilche, F. E. Varela, and L. M. Gassa, "A study of thin anodic WO_3 films by electrochemical impedance spectroscopy," *Electrochimica Acta*, vol. 42, no. 11, pp. 1751–1758, 1997.

[29] J. J. Kim, D. A. Tryk, T. Amemiya, K. Hashimoto, and A. Fujishima, "Color impedance and electrochemical impedance studies of WO_3 thin films: behavior of thinner films in non-aqueous electrolyte," *Journal of Electroanalytical Chemistry*, vol. 433, no. 1-2, pp. 9–17, 1997.

[30] L. Andrade, S. M. Zakeeruddin, M. K. Nazeeruddin, H. A. Ribeiro, A. Mendes, and M. Gratzel, "Influence of sodium cations of N3 dye on the photovoltaic performance and stability of dye-sensitized solar cells," *ChemPhysChem*, vol. 10, no. 7, pp. 1117–1124, 2009.

[31] J. Bisquert, M. Grätzel, Q. Wang, and F. Fabregat-Santiago, "Three-channel transmission line impedance model for mesoscopic oxide electrodes functionalized with a conductive coating," *Journal of Physical Chemistry B*, vol. 110, no. 23, pp. 11284–11290, 2006.

[32] G. Franco, J. Gehring, L. M. Peter, E. A. Ponomarev, and I. Uhlendorf, "Frequency-resolved optical detection of photoinjected electrons in dye-sensitized nanocrystalline photovoltaic cells," *Journal of Physical Chemistry B*, vol. 103, no. 4, pp. 692–698, 1999.

[33] F. Fabregat-Santiago, E. M. Barea, J. Bisquert, G. K. Mor, K. Shankar, and C. A. Grimes, "High carrier density and capacitance in TiO_2 nanotube arrays induced by electrochemical doping," *Journal of the American Chemical Society*, vol. 130, no. 34, pp. 11312–11316, 2008.

[34] R. Kern, R. Sastrawan, J. Ferber, R. Stangl, and J. Luther, "Modeling and interpretation of electrical impedance spectra of dye solar cells operated under open-circuit conditions," *Electrochimica Acta*, vol. 47, no. 26, pp. 4213–4225, 2002.

[35] T. Hoshikawa, M. Yamada, R. Kikuchi, and K. Eguchi, "Impedance analysis of internal resistance affecting the photoelectrochemical performance of dye-sensitized solar cells," *Journal of the Electrochemical Society*, vol. 152, no. 2, pp. E68–E73, 2005.

[36] A. Labidi, C. Jacolin, M. Bendahan et al., "Impedance spectroscopy on WO_3 gas sensor," *Sensors and Actuators B*, vol. 106, no. 2, pp. 713–718, 2005.

[37] M. Pourbaix, *Atlas of Electrochemical Equilibria in Aqueous Solutions*, vol. 282, National Association of Corrosion Engineers, Houston, Tex, USA, 1974.